Chem Soc Rev

Post-Synthetic Modification of Porous Organic Cages

Journal:	*Chemical Society Reviews*
Manuscript ID	CS-SYN-09-2020-001142.R2
Article Type:	Tutorial Review
Date Submitted by the Author:	09-May-2021
Complete List of Authors:	Wang, Hailong; Beijing Key Laboratory for Science and Application of Functional Molecular and Crystalline Materials, Department of Chemistry, University of Science and Technology Beijing, Jin, Yinghua; University of Colorado, Chemistry and Biochemistry Sun, Nana; University of Science and Technology Beijing, Chemistry Zhang, Wei; University of Colorado at Boulder, Department of Chemistry and Biochemistry Jiang, Jianzhuang; University of Science and Technology Beijing, Chemistry

Tutorial reviews

Post-Synthetic Modification of Porous Organic Cages

Hailong Wang,[a,†] Yinghua Jin,[b,†] Nana Sun,[a] Wei Zhang[b,*] and Jianzhuang Jiang[a,*]

Received 00th January 20xx,
Accepted 00th January 20xx

DOI: 10.1039/x0xx00000x

Porous organic cages (POCs) represent an emerging class of organic materials with intrinsic porosity. They have shown various applications in supramolecular chemistry, materials science, and many other related disciplines, which stem from their molecular host-guest interactions, intrinsic and inter-cage porosity in solid state as well as the diversity of functionalities. Post-synthetic modification (PSM) has emerged as a highly viable strategy for broadening the functions and applications of POCs. Intricate structures, enhanced stability, tunable porosity and guest binding selectivity and sensitivity have been realized through PSM of POCs, which cannot be directly achieved *via* the predesign and bottom-up assembly from small molecule building blocks. For example, an unstable imine-linked POC can be transferred to a more stable amine-linked cage, whose cavity size can be further tuned by selective tying of some amine groups, offering unusal gas adsorption selectiviey for noble gases (e.g., preferred uptake of Xe over Kr). Such improvement of the chemcial stability and gas separation properties through the consolidation of linkage and adjustment of porosity is challenging to achieve otherwise. In this tutorial review, we highlight the importance and impact of PSM in engineering the properties of POC molecules, their frameworks, and composites going beyond the direct predesign synthetic strategy. The primary PSM strategies for exploring new compositions, functions and applications as well as their structure-property relationship have been summarized, including cage-to-cage transformation at molecular level, covalent or noncovalent assembly of POCs into frameworks, and formation of composites with guest species or other additives encapsulated.

1. Porous organic cages (POCs) with distinct structural characteristics have been employed as a novel class of versatile nanosized synthons.
2. Various cages can be transformed into new cages with excellent chemical stability and novel properties and functions.
3. Numerous chemical methods can be utilized to transform cages into framework structures, enabling more efficient use of inter-cage porosity.
4. Immobilization/growth of functional guest species can be directed by cages, affording multifunctional materials used in catalysis and energy storage.
5. Challenges and perspectives in post-synthetic modification of POCs towards practical use.

Introduction

Porous organic cages (POCs) are discrete covalent-bonded molecular architectures that exhibit precisely controlled structures, functionalities, and confined nano-sized cavities with multiple open windows in specifically designed geometry and dimension.[1-3] The open windows of the cavities for these POCs allow guest species (e.g., ions and small molecules) to enter and pass through, enabling numerous applications in molecular recognition,[4] sensing,[5] catalysis,[6] separation[7] and storage.[8] The geometry of organic linkers, in combination with covalent bond connectivity, enables the generation of POCs with different physical dimensions, symmetry and topology. POCs have been prepared from multiple organic building blocks by thermodynamically controlled one-step cyclooligomerization or kinetically controlled approaches involving multistep chain elongation reactions and final intramolecular cyclization. The recent advances in dynamic covalent chemistry (DCvC) have enabled highly efficient one-step covalent assembly of POCs from simple organic building blocks. DCvC deals with dynamic covalent bonds, which can reversibly break and reform, similar to supramolecular interactions. Therefore, POCs can be predominantly formed at equilibrium under thermodynamically controlled conditions through error correction and error proof if they are designed to be the most energy favoured strain-free species. With the advent of DCvC,[9-11] POCs have been further enriched in terms of dimension, composition and topology and a variety of fascinating molecular architectures and their applications have been demonstrated.[12-19] Although spectacular research progress has been achieved, thus far the synthesis of POCs through DCvC approach has been mainly limited to highly symmetrical polyhedra (e.g., T_d or O_h symmetry) made of two or three types of building blocks. For bicomponent POCs, they are usually named as a [m+n] POC, which shows the number (m, n) of two organic building blocks composing the POC structure and also the possible topology. For example, a [4+6] POC

[a] *Beijing Advanced Innovation Center for Materials Genome Engineering, Beijing Key Laboratory for Science and Application of Functional Molecular and Crystalline Materials, Department of Chemistry, School of Chemistry and Biological Engineering, University of Science and Technology Beijing, Beijing 100083, China, E-mail: jianzhuang@ustb.edu.cn*
[b] *Department of Chemistry, University of Colorado Boulder, Boulder, Colorado 80309, United States, E-mail: wei.zhang@colorado.edu*
† These two authors contribute equally
Electronic Supplementary Information (ESI) available: [details of any supplementary information available should be included here]. See DOI: 10.1039/x0xx00000x

represents a bicomponent cage likely with a tetragonal D_{4d} topology consisting of four vertices and six edges.

With excellent chemical stability, internal porosity and rich functionalities, POCs have gradually evolved into a novel class of nanosized synthons. POCs usually have good solubility and high purity, thus are expected to be easily covalently or noncovalently assembled into functional materials and devices through solution processing. Their prominent solution processability and atomically precise structural control are even on par with those small molecular synthons. POCs can undergo various covalent and noncovalent chemical reactions, so called post-synthetic modification (PSM), to form functional derivatives with preserved porosity ranging from discrete molecules to covalent-bonded or supramolecular assemblies and further to various composites. Therefore, PSM of POCs can effectively introduce new functions and broaden the functional scope of these discrete porous entities for advanced applications in materials science, biotechnology and many other related disciplines. This tutorial review summarizes the recent progress in the development of cage molecules, cage-derived frameworks, hybrid composites, and property engineering and highlights the great potential of PSM going beyond the conventional predesign and synthesis of POCs.

Hailong Wang

Hailong Wang was born in Jilin, China. He received BSc (2007), MSc (2010) and PhD (2013) degrees from Northeast Normal University, Shandong University and University of Science and Technology Beijing (USTB), respectively, under the supervision of Prof. Jianzhuang Jiang. During 2013–2018, as a postdoctoral fellow, he worked with Prof. Banglin Chen at University of Texas at San Antonio and Prof. Qiang Xu at National Institute of Advanced Industrial Science and Technology. Now, he works at USTB, focusing on porous molecular crystals and tetrapyrrole-based crystalline materials.

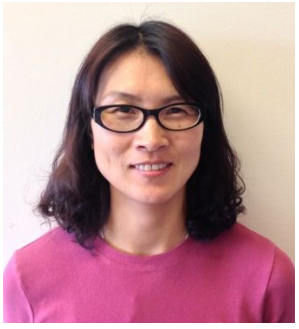

Yinghua (Alice) Jin

Yinghua (Alice) Jin received her B.S. in Chemistry from Peking University in 2000. She obtained her Ph.D. in Chemistry under the supervision of Prof. Robert M. Coates from University of Illinois at Urbana-Champaign in 2006. Her research interests include development of novel organic functional materials and their applications in energy and biomedical fields.

Nana Sun

Nana Sun was born in Henan, China. She received BSc (2012) and MSc (2016) from University of Science and Technology Beijing under the supervision of Prof. Dr. Jianzhuang Jiang. Now, her research interest focuses on both porous organic cages, covalent organic frameworks and supramolecular self-assembly.

Wei Zhang received his B.S. in Chemistry from Peking University in 2000, and his Ph.D. in Chemistry from University of Illinois at Urbana-Champaign (UIUC) in 2005. After a postdoc stint at MIT, he started his independent career at the Department of Chemistry and Biochemistry at University of Colorado Boulder in 2008, and was promoted to Associate and Full Professor in 2014 and 2018, respectively. His research is focused on utilizing dynamic covalent chemistry to develop novel organic and hybrid functional materials targeting a broad range of environmental, energy and biological applications.

Jianzhuang Jiang

Jianzhuang Jiang received his BSc, MSc and PhD (with Tsinglien Chang) from the Peking University in 1985-1993. During 1990-1992, he studied at the Osaka University under guidance of Kenichi Machida and Ginya Adachi. He became a postdoctoral fellow at the Peking University with Zizhao Gan and Chinese University of Hong Kong with Dennis. K. P. Ng and Thomas C. W. Mak and a Visiting Scholar at the Queensland University of Technology with Dennis P. Arnold. He joined the Shandong University and University of Science and Technology Beijing in 1996 and 2008, respectively. He has been working on tetrapyrrole-based functional materials.

Cage-to-cage post-synthetic modification

PSM based on dynamic covalent chemistry

It is well-known that DCvC provides a powerful toolkit for programming functional building blocks into predesigned structures based on the geometry of organic linkers and

connection nodes as well as bonding reversibility.[9-11] More importantly, DCvC allows the error correction during the preparation process, providing the most thermodynamically favored species at equilibrium. So far, many DCvC reactions including imine formation, boronic acid condensation and alkyne metathesis have been utilized in the construction of covalent organic frameworks (COFs), macrocycles and POCs. The dynamically reversible characteristic of DCvC also enables the cage-to-cage PSM.

In 2010, the Cooper group reported the first example of conversion of a monomeric cage to its interlocked dimer through dynamic imine chemistry. The reaction of 1,3,5-benzenetrialdehyde (**1**) with ethane-1,2-diamine (**2**) in the absence of trifluoroacetic acid (TFA) provided the monomeric [4+6] organic cage **3** with four windows and four trialdehyde-units located at tetrahedral vertices (Fig. 1). Interestingly, the monomeric cage **3** in T_d symmetry was able to slowly transform into the crystalline interlocked dimer **4** in *p*-xylene over a period of 50 days in the absence of any templates and catalysts (Fig. 1).[13] According to the single crystal X-ray diffraction analysis, two sets of independent [4+6] tetrahedral cages were interlocked with each other through three windows. The interlocked cage can also be formed as a crystalline solid directly from the monomer solution of **1** and **2** when the catalyst TFA was added. Both monomeric and interlocked cages were found to be stable in air for a long period of time. The interlocked cage is constantly removed out of the reaction solution via crystallization, thus driving the equilibrium movement towards its formation. The transformation of the monomeric cage **3** into the interlocked **4** indicates the interlocked cage was the energy-favored polymorph due to the minimized empty space (densest packing) and the presence of strong intramolecular π···π interactions for the solid sample.

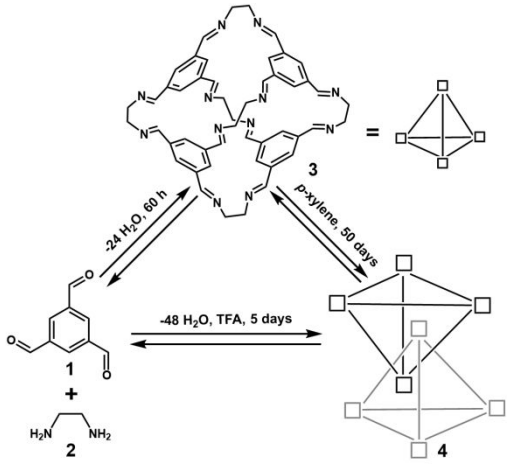

Fig. 1 Synthesis of [4+6] cage **3** and the conversion to the interlocked dimer **4**.

Another example of interlocked organic cage with well-defined crystal structure was reported by the Mastalerz group.[14] It was also formed from the monomeric cage in a high yield of 62% during the crystallization *via* slow vapor diffusion of *n*-hexane into its chloroform solution. The conversion was proceeded by the reversible boronic ester bond breaking and reformation. The transformation was shown to be sensitive to the substituent effect. The interlocked cages containing ethynylene linkages have also been reported by Zhang and coworkers.[15] In contrast to the imine or boronic ester-linked interlocked cages, the ethynylene-linked interlocked cages were formed in a solution phase from the monomer building blocks through dynamic alkyne metathesis under thermodynamically controlled equilibrium conditions. Therefore, such cage formation pathway is different from that for the aforementioned imine-linked or boronic-ester interlocked cages formed as solid precipitates through the conversion of the monomeric cages during crystallization, which likely involves a balanced thermodynamic and kinetic process.

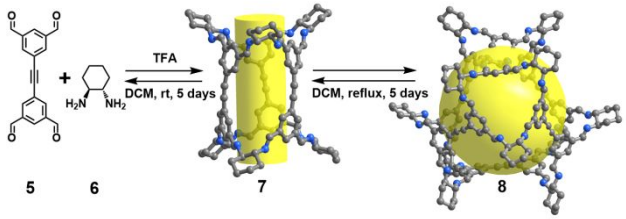

Fig.2 Synthesis of [3+ 6] cage **7** and its rearrangement to [6 + 12] cage **8** (C: grey; N: blue; hydrogen atoms are not shown in crystal structures).

In addition to the formation of interlocked dimer cages, the rearrangement of the topology of a monomeric cage during re-crystallization was also reported.[16] The [3+6] trigonal prism **7**, obtained from the reaction between 5,5'-(ethyne-1,2-diyl)diisophthalaldehyde (**5**) and enantiopure cyclohexane-1,2-diamine (**6**), can transform into the [6+12] truncated tetrahedron **8** during crystallization process (Fig. 2). The formation of the larger [6+12] cage from the [3+6] monomeric cages required the imine bond cleavage and reformation in a suitable solvent medium. According to the molecular simulation, the [6+12] cage is less energetically favoured compared to the [3+6] cage. Such transformation is therefore likely due to the effect of solvation and kinetic factors (e.g., precipitation). The rearrangement was hard to control due to its sensitivity to the cage species, solvents, and catalysts, further indicating there is only a small difference in energy between the formation of large and small cages. Nevertheless, such cage-to-cage topology transformation triggered by the solvent and catalyst could be envisioned as a useful synthetic tool for novel porous materials with innovated functions.

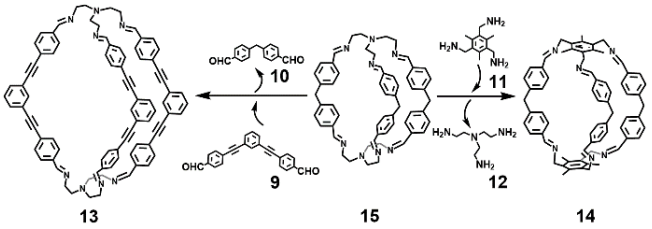

Fig. 3 Conversion the cage **15** to **13** and **14** through dynamic imine reactions.

The third type of cage-to-cage transformation enabled by DCvC is the exchange of cage components based on self-recognition principle.[17] In 2013, the Mukherjee group reported the preferred formation of two cages, **13** and **14** out of the four possible cages at the equilibrium from the mixture of four monomers: two types dialdehydes **9** and **10** and two kinds of triamines **11** and **12** (Fig. 3). The crucial thermodynamically-

controlled self-recognition mechanism discriminated the formation of the less energy-favored cage **15** and another cage consisting of monomers **10** and **12**. The self-recognition capability of these building blocks promoted the cage-to-cage transformation. For example, **15** can be converted to **13** through the replacement of the dialdehyde moiety **10** with **9** (Fig. 3). Similarly, **15** can also be transformed to **14** through the replacement of triamine moiety **12** with **11** (Fig. 3). These examples highlight the power of DCvC in dynamically controlling the product distribution based on the energy landscape.

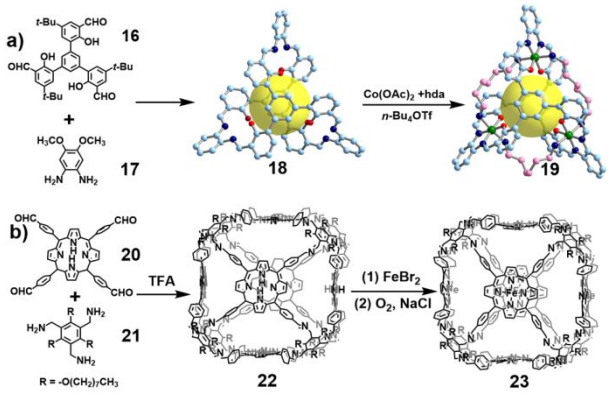

Fig. 4 Modification of cages through metal coordination: (a) Synthesis of cage **18** and its conversion to metal-coordination cage **19** (*n*-Bu_4OTf = tetrabutylammonium trifluoromethanesulfonate; hda = 1,6-hexanediamine; N: dark blue; O: red; C: cyan; Co: green; hda C: pink; Methoxy and selected hydrogen atoms are not shown in these structures); (b) Synthesis of cage **22** and its conversion to metal-coordination cage **23**.

PSM based on coordination chemistry

The excellent stability of covalent molecular cages offers the opportunity of introducing metal-ligand coordination bonds through PSM strategy without causing any structural damage to the cages. The resulting POCs would have covalently bonded, purely organic backbone structures with metal ions located at the surrounding panels or vertices. Therefore, such metal-containing POCs distinguish themselves from common metal organic polyhedra, which are formed from organic linkers and metal-based secondary building units (SBU) through metal-ligand coordination, and usually have higher chemical stability. In addition, through PSM strategy, accessible metal centers coordinated with multiple different functional moieties can be introduced into POCs, which could potentially offer interesting properties originating from such heterogeneity. As shown in Fig. 4a, reversible metal-ligand coordination bonds were introduced through PSM of triangular prismatic POC **18** prepared from imine condensation of trialdehyde monomer **16** and diamine monomer **17**.[18] Reaction of **18** with cobalt(II) acetate and a bifunctional ligand, 1,6-hexanediamine (hda), afforded the metal-containing POC **19** $[LCo_3(hda)_3](OTf)_3$ (L denotes for POC **18**), which displays three octahedral cobalt(III) ions coordinated with two imines, two phenols and two amines in a triangular arrangement. Through the PSM, a 27-membered $(Co\text{-}hda)_3$ macrocycle was formed, which effectively blocks the open window of the cavity of **19**, forming a *closed* cage. Through the similar PSM strategy, an *open*-cage analogue of POC $[LCo_3(MeNH_2)_6](OTf)_3$, where the three hda ligands were replaced by six methylamine ligands, was also be obtained. The ion encapsulation measurements in such *open* cage show the binding constant in the order $Na^+ << K^+ < Rb^+ < Cs^+$. The high affinity of the *open* cage towards Cs^+ and Rb^+ was associated with the rich phenoxy groups of the cage. In contrast, the gate-blocking effect of the *closed* cage severely slowed down its binding kinetics. The adjustment of the window size through PSM of POCs *via* coordination chemistry therefore could harness the gate-effect of POCs for separation applications.

Post-metalation of POCs is also able to provide new catalysts, which can possess highly accessible, catalytically active sites in a porous discrete entity. Due to the porosity, high chemical stability and solution stability of covalent organic cages, these POC-based catalysts have many advantages, including easy accessibility of active sites, facilitated substrate diffusion, and minimized aggregation of catalytic centers.[19,20] For example, the post-synthetic metalation of porphyrin box **22** constructed from **20** and **21** provided the metal-containing POC **23** equipped with six Fe-porphyrin units (Fig. 4b), which can act as active sites for electrochemical reduction of CO_2.[20] The excellent stability of POC **22** enabled the complete metalation with the conservation of the cage structure. The porosity of Fe-containing cage **23** was evidenced by the modest CO_2 uptake of 5.85 wt% at ambient temperature and the Brunauer–Emmett–Teller (BET) surface area of 490 $m^2\ g^{-1}$ calculated from CO_2 sorption isotherms at 195 K. POC **23** showed excellent catalytic activity in electrochemical CO_2-to-CO conversion. Selective production of CO over H_2 with near-quantitative Faradaic efficiency and high turnover number (TON) of 55250 (24 h) was observed in an aqueous solution with a pH value of 7.3. Provided high porosity and spatially well-isolated active sites, **23** exhibited significantly enhanced catalytic activity compared to the six molecular equiv. monomeric iron tetraphenylporphyrin (Fe-TPP) catalyst. The percentage of electrochemically active iron centers in **23** was 1.5 times higher than that in Fe-TPP, providing a larger current intensity, turnover number, and turnover frequency. The higher catalytic activity of **23** than Fe-TPP can be attributed to its porous structure, which minimizes the catalytic center aggregation, exposes more active sites, and facilitates the mass transfer of the substrate and electrolyte.

PSM based on synthetic organic chemistry

Synthetic organic chemistry (irreversible) has been employed for PSM of POCs to directly introduce functional groups that are hard to install through the bottom up synthesis.[21-26] One of the early examples of PSM of POCs is the reduction of imine-linked cages to quench the reversibility of imine bonds and enhance the stability.[21] An imine-linked POC **26** was obtained through one-pot assembly of anthracene-1,8-dicarbaldehyde (**24**) and hexyl substituted triamine **25**, which was reduced to amine-linked POC **27** (Fig. 5a).[21] Single-crystal X-ray analysis clearly revealed the trigonal prismatic structure of cage **27** composed of six amine bonds. The dimension of the central void was estimated to be 21.4 Å x 21.4 Å x 5.6 Å. Such PSM of the imine-linked POC **26** into an amine-linked derivative **27** increased the

CO_2/N_2 adsorption selectivity (1.0 bar and 293 K) from 39:1 to 73:1 owing to the enhanced bonding interactions between amino groups and CO_2 molecules.

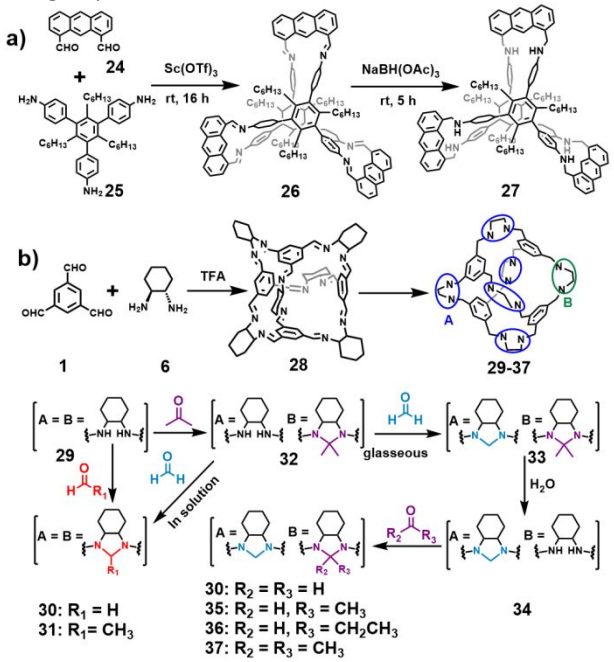

Fig. 5 PSM of cages based on imine/amine chemistry: (a) Reduction of anthracene-containing POC **26** to give **27**; (b) Synthesis of POC **28** and the conversion to various derivatives (**29**-**37**).

The reduction of imine cages into amine counterparts introduces molecular flexibility and thus dramatically deteriorates the shape-persistency and permanent porosity. Such phenomenon was observed when the chiral imine cage **28** (also called CC3) constructed from **1** and **6** was reduced to the amine cage **29** (also called RCC3) (Fig. 5b).[22] Although CC3 is porous even at amorphous state, RCC3 does not exhibit any porosity possibly due to the collapse of the pore structure. However, the chemistry of cyclohexanediamine groups enabled the rich PSM of **29**. Formaldehyde as the smallest carbonyl reagent was utilized to modify the cage **29** at 70°C in methanol, generating **30** consisting of six cyclic aminal moieties as a white precipitate. Such transformation restored the shape persistency and porosity of the cage. The BET surface area of the crystalline **30** was determined to be 377 $m^2\ g^{-1}$, which was slightly lower than that of parent cage CC3 (**28**, 409 $m^2\ g^{-1}$). The crystallinity of **30** remained unchanged even after being activated under dynamic vacuum for 12 h at 80°C or being soaked in acidic (pH = 1.7) or basic (pH = 12.7) solution for 12 days, demonstrating its excellent chemical and crystalline stability. Similarly, **29** was also able to be converted to another cage derivative **31** with six cyclic aminal moieties by reacting with acetaldehyde.[23] Interestingly, when **29** was exposed to acetone, only one vertex diamine was modified, yielding the product **32** as prism-shaped single crystals.[22] This newly formed cage **32** was revealed to contain only one 5-membered imidazolidine ring at a diamine vertex due to the steric hindrance that inhibited further modification of the cage molecule. The mono aminal-substituted **32** had the low BET surface area of 67 $m^2\ g^{-1}$, but exhibited the high thermal and chemical stability, maintaining its crystallinity even after heating at 300 °C and soaking in water for 48 h.

The PSM of the other five empty diamine vertices in **32** provided the opportunity to fine-tune the internal cavity of POCs.[23] For example, the reaction of **32** with gaseous formaldehyde led to a single-crystal-to-single-crystal transformation to **33** with dual "ties", namely one isopropyl-tied aminal and five methylene-tied aminals (Fig. 5b). The isopropyl-substituted aminal of **33** was selectively hydrolyzed to generate **34** with one free diamine group, which can be further functionalized with various aldehydes (e.g. formation of **30**, **35**-**37** shown in Fig. 5b). Such easy PSM method was able to finely tune the pore size of the cage molecules and thus the gas adsorption selectivity of solid assemblies. These post-modified POCs showed interesting adsorption behaviors towards Xe and Kr, which is known extremely challenging to separate. Most of the RCC3 derivatives displayed the higher uptakes for Xe than Kr. However, reverse Kr/Xe uptake selectivity was observed for **35** owing to its pore size that matches well with the size of Kr but is too small for Xe. Provided a pore size close to the minimum molecular dimension of H_2 (2.2 Å), **31** has also shown a great potential for hydrogen isotope separation. Cryogenic thermal desorption spectroscopy (TDS) measurement of **31** unveiled its excellent D_2/H_2 separation selectivity of up to 3.9 with a low D_2 adsorption capacity of 0.8 mmol g^{-1} at 30 K. An optimal dual-cage cocrystal composed of **31** and CC3 was used to improve the quantum sieving performance with a high D_2/H_2 separation selectivity of 8.0 and a deuterium uptake of 4.7 mmol g^{-1}. The former cage exerted the kinetic quantum sieving effect to block H_2 diffusion and the latter species possesses larger porosity for gas adsorption.

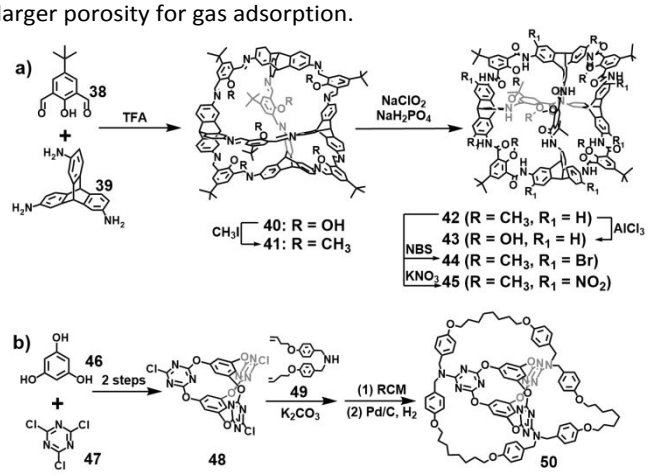

Fig. 6 PSM of cages through substitution, oxidation/reduction and metathesis reactions: (a) Synthesis of POC **40** and its conversion to the derivatives; (b) Synthesis of POC **48** and its modification to form a molecular barrel **50**.

Later, the post-synthetic fine-adjustment of the molecular aperture of POCs has also been reported by Mastalerz and co-worker.[24,25] An adamantoid imine cage **40** was prepared from 5-(*tert*-butyl)-2-hydroxyisophthalaldehyde (**38**) and 2,6,14-triaminotriptycene (**39**) through imine condensation (Fig. 6a). The cage intrinsic porosity was tuned by methylation, giving a new fully methylated cage **41** (Fig. 6a).[24] Single crystal X-ray

diffraction analysis of **41** clearly disclosed the presence of six methyl carbon atoms with an average edge distance of 8.53 Å inside the cage. This PSM strategy was able to be extended towards preparing propyl-, allyl-and benzyl-substituted cages in isolated yields above 60%. The nitrogen adsorption isotherms at 77 K revealed the gradual decrease of the BET surface area with the increased size of the substituents. Compared with the BET surface area of 2071 $m^2 g^{-1}$ of the crystalline **40** sample, the BET surface area of the cage **41** was much lower regardless of the activation conditions (741-1700 $m^2 g^{-1}$). Despite the slight difference in the CO_2 adsorption between the parent cage **40** (60.2 $cm^3 g^{-1}$, 1.0 bar, 273 K) and the modified derivative **41** (56.3 $cm^3 g^{-1}$), almost five times higher adsorption heat (60.6 kJ mol^{-1} *vs.* 12.2 kJ mol^{-1}) was calculated for the former cage due to the favored binding interactions of the hydroxy moieties with the CO_2 molecules. PSM protocols are very effective for providing POCs with high chemical stability for practical applications. A chemically robust amide cage **42** was prepared by utilizing a Pinnick oxidation reaction of **41** (Fig. 6a).[25] This amide cage can tolerate acidic and basic aqueous solution (pH = 1-14.5) and even harsh PSM process in the presence of Lewis-acid $AlCl_3$ and trifluoracetic acid. As a result, demethylation, bromination and nitration at the triptycene moieties provided the new cage derivatives **43**-**45**, respectively (Fig. 6a). Compared with the parent cage **42**, the nitro-containing cage **45** showed notably improved CO_2/CH_4 sorption selectivity (Henry selectivity of 28 *vs.* 20) and increased CO_2 adsorption heat (35 kJ mol^{-1} *vs.* 26 kJ mol^{-1}).

The Wang group reported an interesting approach to prepare a molecular barrel through PSM of a shape-persistent cage.[26] As shown in Fig. 6b, a D_{3h} symmetric organic cage **48** was assembled by a two-step reaction from phloroglucinol (**46**) and cyanuric chloride (**47**). The three chloro groups of cage **48** could be easily replaced by the amino group of **49** through nucleophilic aromatic substitution. The resulting intermediate equipped with two terminal olefin groups underwent ring-closing metathesis (RCM) followed by hydrogenation of the olefin moieties to form a molecular barrel **50** with a 63-membered loop. Single crystal X-ray diffraction structure of **50** revealed that three new outer molecular cavities were grafted around the center cage. Although the parent cage **48** did not show noticeable CO_2 uptake, the amorphous solid sample of molecular barrel **50** exhibited a moderate CO_2 uptake (28.1 $cm^3 g^{-1}$ of CO_2 at 273 K and 1.0 bar) with a high isosteric enthalpy (36 kJ mol^{-1} at zero coverage) due to the existence of rare lone pair-π interactions between the electron-deficient triazine moiety and CO_2 molecules according to the IR characterization and theoretical simulations.

The PSM strategy using the dynamic covalent chemistry, metal-ligand coordination and synthetic organic chemistry has been demonstrated to successfully realize cage-to-cage transformation. Tuning the chemical structures of POCs directly impacts their robustness, stability and functions. DCvC strategy provides a powerful tool to construct shape-persistent POCs, which, however, is a double-edged sword due to the introduction of reversible bonds, leading to inferior chemical stability for practical applications. It is worth noting that the ligand-exchange may open many possibilities for imparting new functionalities to POCs. In addition, reversible metal-ligand coordination strategy can introduce Lewis acidic metal centers with diverse catalytic activities and emission nature. The stabilization through the synergistic effect of coordination bonds and covalent bonds consolidates the molecular rigidity of POC, which could be beneficial for host–guest interactions, light-harvesting, and sensing. Through rich synthetic organic transformation, labile bonds within POCs can be fixed to improve their chemical stability. Precise tailoring of pore size and functionalities has been realized, thus enabling significant applications such as challenging gas separation.

Cage-to-framework post synthetic modification

Cage-to-polymer

Cage-to-framework strategy by utilizing POCs as the synthons to construct covalent polymers was first demonstrated in 2011.[27] A bottom-up cage-to-framework strategy provides an avenue for accessing diverse functional cage-derived porous materials (Fig. 7a). Sonogashira coupling of a trigonal prismatic bromo-substituted cage building block **51** with 1,4-diethynylbenzene (**52**) generated the covalently linked cage-based polymer **53**. The cross-linked polymer **53** exhibited four times higher CO_2 uptake than that of the parent cage at 1.0 bar and 293 K, possibly due to the generation of extra inter-cage porosity. Under the microwave condition, a series of cage-derived organic frameworks with high thermal stability have been prepared through the Sonogashira coupling between **51** and rod-like diacetylene linkers. The gas adsorption properties were tuned through the choice of the linear linkers with different size and functionalities. Superior CO_2/N_2 adsorption selectivity (up to 213/1) was observed when triethylene glycol methyl ether substituent was introduced to the linear linker.

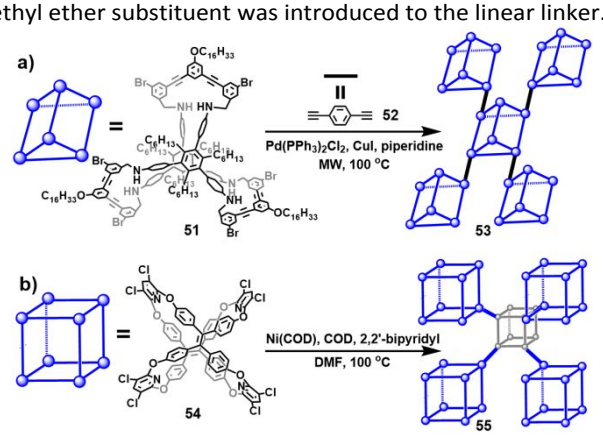

Fig. 7 Covalent crosslinking of POCs **51** and **54** to form polymers **53** and **55**, respectively.

Cage-to-polymer approach is able to effectively enhance the accessibility of the internal cavity of POCs, forming porous materials with both intrinsic and extrinsic cage porosity. The tetraphenylethylene-based oxacalixarene cage **54** (Fig. 7b) prepared from tetrahydroxy-tetraphenylethylene with tetrachloropyridine through S_NAr reaction packs in window-to-arene mode with isolated lattice voids, thus is non-porous. The polymerization of the cage **54** was performed *via* a nickel(0)-

catalyzed Yamamoto-type Ullmann cross-coupling reaction.[28] In the resulting crosslinked-cage polymer **55** (Fig. 7b), the window-to-arene packing was prohibited, thus providing accessibility to the internal pores of the cage. Compared with the monomeric cage, the cage-based polymer **55** showed a significantly enhanced BET surface area of 929 $m^2 g^{-1}$ and CO_2 uptake of 49.3 $cm^3 g^{-1}$ at 273 K and 1.0 bar due to the formation of inter-cage porosity upon polymerization. More interestingly, the polymer **55** displayed a great potential for CO_2 sensing applications. Upon CO_2 uptake, the fluorescence intensity of **55** increased to 211% after 1 min and reached 307% after 5 min. The fluorescence intensity recovered to the original value when CO_2 was released by $NH_3 \cdot H_2O$ treatment. By contrast, the cage **54** did not show any fluorescence change when CO_2 was bubbled into its methanol solution. This phenomenon was explained by the restricted rotation and vibration of phenyl rings of the tetraphenylethylene moieties in **55** due to the rigid framework structure and entrapped CO_2 molecules in the cavity. Although cage-to-framework transformation through polymerization/coupling reaction has been realized, the conversion of cage monomers seems low, likely due to the steric effect.

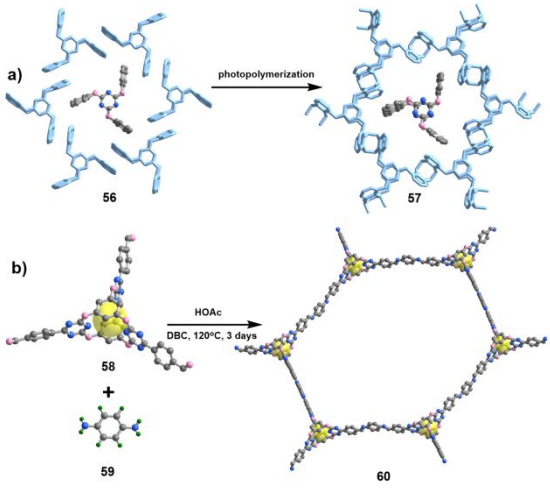

Fig. 8 Cage-to-framework strategy to form covalently linked ordered network polymers: (a) Synthesis of 2DP **57** through solid state photopolymerization of crystalline cage **56**; (b) Synthesis of COF **60** from cage **58**. For the structures, C: grey; O: pink; N: blue; cage void: yellow.

Cage-to-ordered organic framework

In the above cage-to-framework approach, irreversible cross-coupling of cage molecules has been explored, which generally provides amorphous materials with ill-defined structures. Ordered arrangement of cages in a polymeric network is more challenging and requires either the pre-organization of cage precursors prior to polymerization or the covalent assembly of cage-like building blocks through DCvC. Schlüter and co-workers reported the polymerization of the C_3 symmetrical cage-like monomer to form a crystalline covalent-bonded two-dimensional polymer (2DP).[29] Three 1,8-disubstituted anthracene blades were placed in a rigid C_3 symmetric cage molecule **56** with limited conformational freedom and low solubility, which facilitated the crystallization (Fig. 8a). The cage **56** crystalized in a lamellar packing mode with π···π interactions between the neighbouring anthracene units. Such arrangement allowed [4+4]-cycloaddition photodimerization of anthracene moieties to form 2DP **57** (Fig. 8a). Gram scale 2DP **57** was prepared, whose structure was unambiguously revealed by single crystal X-ray diffraction. More importantly, the 2DP crystals could be delaminated into a large amount of nanosheets including single layer sheets, which represents a rare example of 2D ordered architecture with a high structural perfection. In addition, the depolymerization of 2DPs back to the monomers could be realized by heat or irradiation under light with the wavelength < 300 nm.

Recently, POCs have been explored as multivalent vertices in COFs.[30,31] For example, two crystalline cage-based 2D COFs have been prepared through dynamic imine chemistry from cage monomer **58**. As shown in Fig. 8b, the prismatic cage building block **58**, with a C_3-symmetry, reacted with 1,4-phenylenediamine (**59**) through imine condensation under solvothermal conditions to give the crystalline COF **60**.[30] The hexagonal structure of **60** consists of six prismatic cage knots linked by six aromatic linkers. Due to the unique cage-linked structure, the COF layers were packed into a rare A-B-C staggered form rather than the conventional A-A and A-B packing mode. In such packing mode, the stacking interactions of all phloroglucinol faces were maximized. The pore size of **60** was estimated to be *ca.* 1.2 nm according to nitrogen adsorption data at 77 K. In contrast to nonporous nature of the parent cage **58**, the BET surface area of **60** reached 1237 $m^2 g^{-1}$.

Interesting DCvC-enabled cage-to-COF and COF-to-cage transformation has also been realized through the exchange of components in a dynamic system.[32] When imine-linked cage **3** was reacted with **59** under solvothermal conditions (HOAc, 3 days at 120°C) in 1,4-dioxane, cage-to-COF transformation was occurred, providing a crystalline COF, namely COF-LZU-1. The crystalline structure of COF-LZU-1 was confirmed by powder X-ray diffraction characterization. Similarly, COF-to-cage transformation was also observed when a boronic ester linked COF (COF-NUST-1) was reacted with *o*-phenylene diboronic acid. This study highlights the power of DCvC, which effectively differentiates thermodynamically metastable components of a dynamic system and favors the formation of energy-preferred structures.

Cage-to-MOF/HOF

Beside covalent-bonded cage-based polymers, supramolecular frameworks have also been actively pursued by connecting cage synthons through noncovalent interactions. Metal-organic frameworks (MOFs) are a class of crystalline organic-inorganic hybrid porous materials, which have usually been constructed through the assembly of discrete organic ligands and metal ions/clusters by coordination bonding.[33] POCs are also able to serve as unique macromolecular ligands and coordinate with metal ions to form MOFs, opening up new perspectives for introducing extrinsic cage porosity. Alternatively, supramolecular assembly of POCs through hydrogen-bonding interactions can form hydrogen-bonded organic frameworks (HOFs), another type of porous materials

constructed through assembly of organic molecules.[34] In 2010, the first molecular cage-based MOF was reported.[35] This cage-based MOF **62** was obtained by the complexation of divalent zinc ions with RCC1 (**61**) (Fig. 9a). Single crystal X-ray diffraction analysis of **62** showed the amino cage served as a chelating ligand with six bidentate diamine groups to complex with six zinc ions from different hexanuclear zinc carbonate clusters $[Zn_6(\mu_3\text{-}CO_3)_4]^{4+}$. This MOF can thus be regarded as a cationic network with the intrinsic voids of the cages partially occupied by counter anions. Unfortunately, the material was almost nonporous as determined by the nitrogen and hydrogen sorption study at 77 K, which is likely due to the counter ions blocking the void space. Such cage-based MOF can adsorb 0.9 mmol g^{-1} CO_2 at 298 K and 1.0 bar, suggesting the existence of permanent porosity that is selective for CO_2 adsorption. Cage-based MOFs bridge POCs and MOFs, representing a new strategy to prepare MOFs by utilizing predesigned functional cage-like ligands.

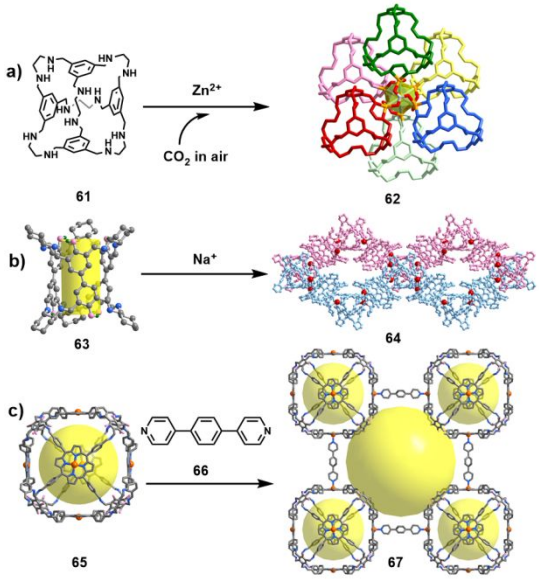

Fig. 9 Cage-to-MOF strategy: (a) Synthesis of MOF **62** from RCC1 (**61**); (b) Synthesis of MOF **64** from cage **63**; (c) Synthesis of MOF **67** from cage **65** (*n*-butyl was not shown in the figure). For these pictures, Zn, orange; C, gray; N, blue; O: pink; H: green; selected hydrogen atoms are omitted for clarity.

The cage-to-framework strategy has inspired a new idea towards constructing hierarchically porous MOFs with 0D internal voids of POCs and 1D or 3D interconnected extrinsic inter-cage channels. As shown in Fig. 9b, a shape-persistent triangular prismatic imine-based cage **63**, which was prepared through a condensation reaction of 3,3',5,5'-tetraformyl-4,4'-biphenyldiol with **6**, has been assembled into MOF **64** with the assistance of excessive NaN_3.[36] The MOF consisted of 1D single-strand helices with the pitch length of 38.917(5) Å, which further assemble through van der Waal interactions into porous supramolecular structure containing both cage intrinsic porosity and extrinsic channels. As a result, MOF **64** shows an improved BET surface area (1230 m^2 g^{-1}) and CO_2 uptake (1093 cm^3 g^{-1} at 23 bar/273 K) compared to those of **63**.

The Kim group also reported hierarchically porous MOFs prepared through the self-assembly of a nanometer-sized shape-persistent zinc-containing porphyrin box **65** (Fig. 9c). Coordination between Zn ions of the cage **65** and bipyridyl-derived organic linkers with the length ranging from 9.4 to 13.6 Å provided MOFs of various pore sizes.[37] However, the rod-like analogues with the length either shorter than 9.4 Å or longer than 13.6 Å all failed to give hierarchically porous MOFs. There is an optimal range of the length of the linkers, which allows interpenetration and π···π interactions between the adjacent conner benzene rings from neighboring cages to form a stable network structure. The crystal structure of MOF **67** assembled from **65** and 1,4-di(4-pyridyl)-benzene (**66**) showed 2-fold interpenetration and two types of voids: the intrinsic cavity of **65** and the extrinsic pore channels. Provided six porphyrins with unique photochemistry per cage, MOF **67** can promote photo-driven $^1O_2$ generation, which can be used in the photooxidation of 1,5-dihydroxynaphthalene to form the natural product, juglone. The catalytic conversion using MOF **67** was much faster than using cage **65** under the same reaction conditions. These results indicate a bright perspective of functional hierarchical porous cage-derived MOFs in the field of catalysis and photodynamic therapy.

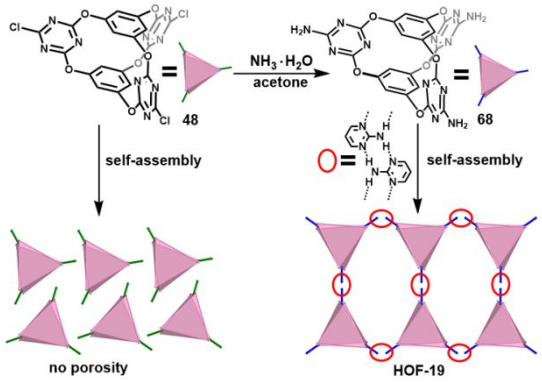

Fig. 10 Synthesis and self-assembly of POC **68** into HOF-19.

HOFs represent an emerging group of crystalline porous materials in addition to MOFs and COFs. In 2019, the first example of cage-based robust HOF-19 was reported. The hydrogen bonding-directed assembly of cage **68** prepared by the substitution of the chloride atoms in **48** with amino groups successfully provided HOF-19 with excellent stability (Fig. 10).[38] Multiple hydrogen bonding interactions between amino and triazine groups as well as the π···π interactions between aromatic moieties of neighboring cage molecules played a critical role in enhancing the stability of the HOF to tolerate non-polar and medium-polar solvents. The porous nature of HOF-19 was determined by the nitrogen sorption at 77 K, giving a BET surface area of 685 m^2 g^{-1}. The rich heteroatoms enabled the post-synthetic metalation of this HOF. Reaction of HOF-19 with $Pd(OAc)_2$ gave a Pd^{2+}-functionalized porous HOF-based catalyst (Pd^{2+}@HOF-19). Such catalyst was able to effectively and selectively promote the Suzuki-Miyaura coupling reaction between aryl halides and phenylboronic acid in high yields (96–98%) due to the well-dispersed Pd^{2+} in the HOF channels and the size exclusive effect of the HOF support. Simple recrystallization was capable of recovering the catalytic activity of deactivated species, showing the unique advantage of HOF-

based catalysts. The use of cages as multivalent synthons that could generate a series of weak stabilizing interactions is critical for the enhancement of robustness of HOFs to resist the solvent dissociation and expand their diverse applications in solution phase.

An interesting supramolecular complexation strategy for POCs should also be mentioned, which led to the formation of porous liquids (PL), instead of solid frameworks.[39] In detail, a simple liquefaction method was established by mixing an anionic analogue of POC **61** with excess amount of dicyclohexano-18-crown-6 (18-crown-6) and dicyclohexano-15-crown-5 (15-crown-5), giving Type I and II porous liquids (Type I porous liquids refer to those neat species made up of sole empty fluid porous substances and Type II refers to dissolved empty porous substances in a solvent[39]), 18-C-6-PL and 15-C-5-PL, respectively. The porous ionic liquids were formed through the interactions between the anionic POC and cationic 18-crown-6/potassium ion complexes. The size of cationic counter species was too big to enter the internal cage cavity, thus the internal porosity of the cage remained available for the accommodation of small guests. The empty cavities in the porous ionic liquids were confirmed by positron annihilation lifetime spectroscopy (PALS) tests. Molecular simulations suggested a slightly larger cage pore size of 18-C-6-PL (4.6 Å) than that of 15-C-5-PL (4.4 Å), which was consistent with the PALS results. The glass transition temperature for 18-C-6-PL and 15-C-5-PL were about 50 °C and 30 °C, respectively. Such simple PSM approach provides the possibility of scale-up design and preparation of porous liquids, instead of a painstaking synthesis.

The cage-to-framework strategy has realized the conversion of cages to polymers, MOFs, COFs, HOFs, and even porous liquids. The POC molecules have been used as powerful building blocks to construct hierarchically porous materials. Through cage-to-framework post-modification, the surface area of POCs can be effectively enhanced by generating extrinsic porosities. In addition, the cage-based materials inherit the original properties of POCs, representing a novel class of advanced functional porous materials.

Cage-to-composite post synthetic modification

POC-Nanoparticle hybrid complex

POCs have recently been explored as a new kind of scaffolds/templates for confined growth of nanoparticles. Metal anchoring sites can be conveniently installed inside the cavity of a cage, which induces metal ion binding, nanocluster nucleation, and further growth of nanoparticles inside the cage. Cage backbone serves as a protecting shell, preventing the agglomeration of nanoparticles. Using a cage as a hosting template, stable ultrafine

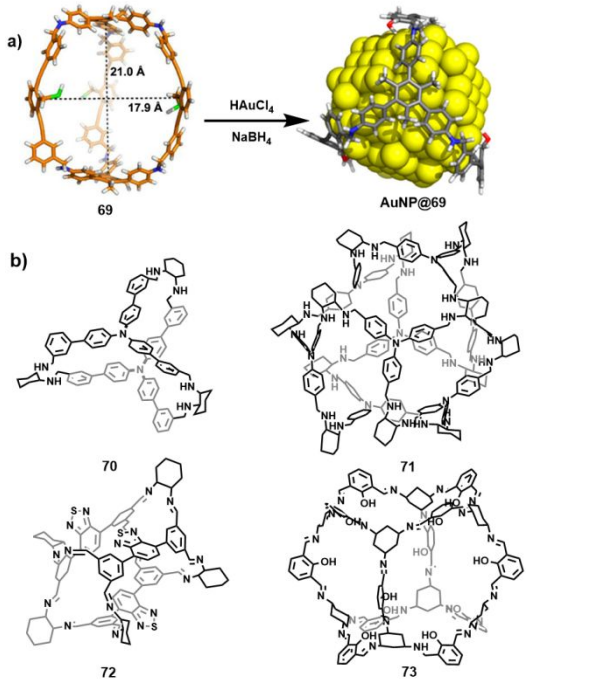

Fig. 11 Cage-templated growth of various nanoparticles: (a) Simulated molecular structure of trigonal prismatic cage **69** and synthesis of AuNP@**69**. Methyl groups for hexyl chains and hydrogen for $OC_{16}H_{33}$, ethyl, and Br were used in the calculation for simplification. Adapted from ref. 40 with permission from the American Chemical Society, copyright 2014; (b) Selected POCs **70**-**73** used as templates for the controlled growth of nanoparticles (t-butyl is not shown in the structure of **73**).

nanoparticles (1-2 nm) have been obtained. For example, a POC was used as a template in the size-controlled preparation of gold nanoparticles (NPs), as demonstrated by Zhang and coworkers in 2014.[40] A C_3 symmetric cage **69** with three thioether groups installed inside the cage was designed and prepared through imine condensation reaction (Fig. 11a). To prepare cage-supported Au NPs (AuNP@**69**), a biphasic mixture consisting of an aqueous solution of $HAuCl_4$ and a CH_2Cl_2 solution of **69** containing a phase-transfer reagent, tetraoctylammonium bromide, was employed to transfer $AuCl_4^-$ from water phase into the organic phase. Then $AuCl_4^-$ was reduced to the cage-supported Au NPs using $NaBH_4$. TEM images revealed an average diameter of 1.9 nm for the narrowly dispersed Au NPs. This is consistent with the cage cavity size of 1.8–2.1 nm. These cage-supported Au particles in AuNP@**69** displayed high solubility in common organic solvents and good stability even after several months, implying the accommodation of the Au nanoparticles inside the cage. Additional evidence for the AuNP encapsulation inside the cage came from the ^1H diffusion-ordered spectroscopy (DOSY) NMR investigation, which shows similar diffusion coefficients for cage **69** and AuNP@**69**, suggesting their similar size and shape. In the control experiments with non-thioether cage or thioether-containing ligand only, aggregated NPs instantly precipitated out upon the addition of $NaBH_4$ due to the lack of nucleation sites and the cage template. Furthermore, the theoretical calculations of the interactions between the cage and AuNPs with different radii showed the total energy minimum when the AuNP size reached to 1.7 nm, which is in close agreement with the experimental nanoparticle size of 1.9 ± 0.4 nm. This work not only

demonstrated the unique confinement effect of a POC and multiple metal-binding sites on controlling the growth of metal NPs with a narrow size distribution, but also afforded an experimental benchmark in systematically characterizing cage-supported metal nanoparticles. Similarly, PdNPs encapsulated in **69** was also obtained with a narrow size distribution (1.8 ± 0.2 nm). Provided a protecting cage shell with minimum surface coverage, such PdNPs were capable of catalyzing organic reactions, showing high catalytic activity and reusability in Suzuki-Miyaura coupling reactions.[41] Diverse POCs and noble metals were then engineered to fabricate cage-supported metal NPs for exploring their catalysis performance,[42-45] opening a new research direction for POCs.

Several cages **28**, **29** and **70**-**73** consisting of vicinal diamine metal binding moieties (Figs. 5b and 11b) have also been explored as templates for the growth of nanoparticles. For example, CC3-*R*, namely an enantiomer of **28**, was applied to stabilize Rh NPs.[42] A mixture of CC3-*R*-containng dichloromethane/methanol solution and rhodium acetate was directly reduced by $NaBH_4$ to give a homogenized heterogeneous catalyst Rh/CC3-*R*-*homo*, which was dissolved in the solution. The morphology of Rh NPs in Rh/CC3-*R*-*homo* with the average diameter of 1.1 ± 0.2 was well characterized by high-angle annular dark-field scanning transmission electron microscopy analysis. Only a small portion (~9%) of Rh NPs in Rh/CC3-*R*-*homo* displayed the smaller size than the cage void size of 0.72 nm, suggesting most nanoparticles anchored on the cage surface. The obtained Rh/CC3-*R*-*homo* catalyst was able to efficiently promote the methanolysis reaction over ammonia borane. In particular, the H_2 evolution TOF value (215 mol) for Rh@CC3-*R*-*homo* in methanol was much higher than that for PVP-supported Rh NPs (15 mol) and the heterogeneous catalyst Rh@CC3-*R*-*hetero* (66 mol) prepared by drying a solution of Rh@CC3-*R*-*homo* under nitrogen stream. This work illustrated that POCs could serve as both the stabilizer and dispersing regent for metal nanoparticles to effectively adjust the reaction kinetics, representing a new homogenization strategy of heterogeneous catalysts using a cage support. Later the same group reported the use of cage **29** (RCC3) as a template to grow Pd nanoclusters with precisely controlled size (~0.72 nm) through a reverse double-solvents approach, where a small amount of hydrophobic solvent was used to disperse the metal precursor and a large quantity of hydrophilic solvent was used to disperse the cage.[43] The metal precursors were reduced with a highly concentrated aqueous solution of $NaBH_4$, providing ultrafine nanoclusters encapsulated inside the cage cavities. The resulting Pd@RCC3 hybrid had excellent solubility and dispersibility in solution, high accessible surface area, and high catalytic activity towards various reactions including hydrogenation of 4-nitrophenol, reduction of organic dye molecules, and methanolysis of NH_3BH_3. Pd@RCC3 catalyst exhibited excellent durability and stability.

The Mukherjee group studied the effect of the cavity size of POCs on the growth of metal nanoparticles. Two cages **70** and **71** (Fig. 11b) containing vicinal diamines were prepared through imine condensation from the reaction of **6** with triphenyl amine-based trialdehyde or 4,4',4''-nitrilotribenzaldehyde, respectively, followed by the subsequent reduction reaction.[44] On the basis of DFT simulations, the cavity size of **70** (≤ 2.0 nm) was smaller than that of **71** (*ca.* 2.4 nm). The reduction of $Pd(OAc)_2$ (equimolar amount with cycloheximide groups in the cage supports) by $NaBH_4$ in the presence of the two different POCs gave a soluble material (Pd@**70**) and an insoluble precipitate (Pd@**71**). Although Pd@**70** had palladium nanoparticles of the size ~1.8 nm, consistent with the pore size, the size of Pd particles in Pd@**71** was around 3.7 nm, suggesting the deposition of nanoparticles on the cage periphery instead of the inside cavity. Pd@**70** (2 mol% loading) showed higher catalytic activity than Pd@**71** (4 mol% loading) due to the larger accessible surface area of the smaller Pd NPs.

The pre-installed metal binding sites (e.g. thioether groups, vicinal diamines) and void space of POCs are critical in the synthesis of cage-supported ultrafine metal NPs with high activity for various catalytic transformation of organic molecules. By incorporating other functional moieties into the cage skeleton, organic cages can synergistically participate in catalysis together with NPs rather than playing only a passive role. In a recent report, a multifunctional tubular cage **72** with benzo[*c*][1,2,5]thiadiazole unit (Fig. 11b), which possessed excellent fluorescence property and photocatalytic function, was used as a template for nanoparticle growth to realize a synergistic catalytic effect.[45] The effective and selective binding of the cage with divalent Pd ions induces the specific fluorescence sensing. The addition of $NaBH_4$ into a solution containing palladium acetate and **72** generated ultrafine cage-encapsulated Pd NPs with a size of *ca.* 1.9 nm. Owing to the capability in promoting superoxide radical anion ($O_2^{\bullet-}$) evolution under light irradiation, **72** can act synergistically with the PdNPs encapsulated inside and catalyze multistep chemical transformations. For instance, PdNPs@**72** can efficiently catalyze one-pot two-step cascade reaction from 4-nitrophenylboronic acid *via* a 4-nitrophenol intermediate to 4-aminophenol through the visible light-induced aerobic hydroxylation and subsequent hydrogenation.

POCs with hydrophilic interior cavities can be utilized to accommodate metal oxide nanoparticles. A [12+8] topological organic cage **73** (Fig. 11b) constructed from 4-tert-butyl-2,6-diformylphenol and *cis*,*cis*-1,3,5-triaminocyclohexane was employed to encapsulate ferrihydrite (Fh) nanoparticles.[46] The phenol oxygen and imine nitrogen atoms served as the anchoring sites. At the initial stage, after mixing POC **73** and an excess amount of $FeCl_2{\cdot}4H_2O$ in $MeOH/CH_2Cl_2$ for 24 h under nitrogen, the dominant formation of Fe_8O_4@**73** was observed in the MALDI-TOF-MS spectra. DFT calculations indicated four oxo-bridged dinuclear [Fe_2O] units at the four sets of metal binding sites composed of three *syn*-salicylimine moieties and imine nitrogen and phenol oxygen atoms pointing inside of the cavity. This study clearly showed the importance of metal binding sites installed in the cage at the initial stage of nanoparticle growth, which likely initiate the formation of nuclei and guide their further growth inside the cage. Oxidation of Fe(II) ions by exposing the above mixture to air and then heating at 180 °C provided ferrihydrite (Fh) nanoparticles encapsulated in the cage (Fh@**73**), which was soluble in

common organic solvents. The morphology and composition of Fh@**73** were characterized by various techniques, showing well-dispersed ultrafine 1.9 nm Fh particles. Compared with the suppressed redox activity of the conventional iron oxide nanoparticles in an organic solvent, the soluble Fh@**73** in CH_3CN exhibited substantial redox activity originating from the ultrasmall metal oxide particles encapsulated by the cage.

Other POC-based composites

Given the excellent chemical and thermal stability, unique pore topologies and solution processability, POCs hold great potential as charge carriers especially when combined with inorganic salts. The Cooper group demonstrated that the amine cage RCC1, which was prepared from the reduction of **3** with $NaBH_4$, can form crystalline salts in the presence of dilute HCl or H_2SO_4 solution.[47] Single crystal X-ray diffraction study revealed that the salts, $(H_{12}RCC1)^{12+}\cdot12Cl^{-}\cdot4(H_2O)$ and $(H_{12}RCC1)^{12+}\cdot6(SO_4)^{12-}\cdot27.25(H_2O)$, possessed twelve protons located on the six amino groups of each cage molecule, which were balanced by twelve chloride ions or six sulfate anions located around the cage window. The cavity was filled with water molecules and the three-dimensional hydrogen-bonded network was formed by chloride/sulfate anions, $(H_{12}RCC1)^{12+}$ cations and H_2O molecules. The cage salt $(H_{12}RCC1)^{12+}\cdot12Cl^{-}\cdot4(H_2O)$ exhibited excellent proton conductivity as high as *ca.* 1.0×10^{-4} S cm^{-1} at low relative humidity (30 % RH), similar to that of commercial Nafion.

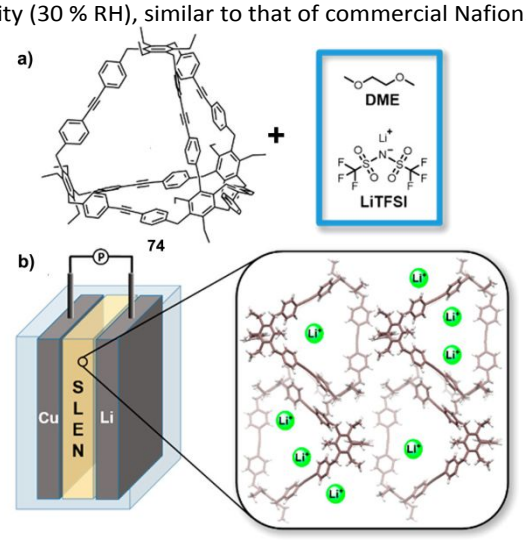

Fig. 12 (a) Structures of the nanocomposites components including cage **74** and LiTFSI and (b) configuration of half-cell. Adapted from ref. 48 with permission from the American Chemical Society, copyright 2018.

POC-inorganic salts combination has also been confirmed as a good lithium-ion conductor. The cage **74** prepared via alkyne metathesis of a 1,3,5-tribenzyl-2,4,6-triethylbenzene derivative was used in combination with 1 M bis(trifluoromethane)-sulfonamide lithium salt (LiTFSI) in 1,2-dimethoxyethane to form a solid-liquid electrolyte nanocomposite (SLEN) (Fig. 12).[48] The SLEN composite exhibited excellent room temperature lithium-ion conductivity of 1.0×10^{-3} S cm^{-1} with a low activation barrier of 0.16 eV and high oxidative stability (up to 4.7 V *vs.* Li/Li$^+$). Both the cage and trapped solvent components were shown to play important roles in the conduction of lithium ions. The use of the cage precursor only under the same conditions displayed inferior conductivity performance.

POCs have been used as a new class of supports to accommodate diverse functional guests using various nanomaterial preparation methods. The intrinsic porosity and heteroatomic composition of POCs exert diverse roles in the guest-impregnation and applications, such as providing metal nucleation sites, serving as dispersing and templating regents and stabilizers for metal nanoparticles. The resulting cage-supported metal nanoparticles exhibit narrow size distribution, high catalytic activity, and stability. In addition to nanoparticles, metal oxides, Brϕnsted acids, and lithium ions have been complexed and combined with POCs to form functional cage-based composite with solution processibility. Compared with conventional insoluble polymer-based composites, many cage-based composites are soluble, thus can be characterized by various spectroscopy techniques, which can provide a deep insight into the interaction between the cage host and guest species.

Table 1. A summary of the PSM of selective POCs.

POC	PSM method	Reactive groups (It has)
3, 7, 15	DCvC	dynamic imine bonds
18	CC	metal binding N_2O_2 sites
22	CC	metal binding N_4 sites
26, 28	SOC	unsaturated imine groups
29	SOC	reactive amine groups
40	SOC	reactive hydroxyl groups
41	SOC	oxidizable imine groups
42	SOC	reactive methoxy groups
43	SOC	reactive aromatic rings
48	SOC	reactive aromatic chloro substituents
51	CP	reactive aromatic bromo substituents
54	CP	reactive aromatic chloro substituents
56	CO	photoactive anthracene groups
58	CO	reactive aldehyde groups
3	CO	dynamic imine groups
61	CM	metal chelating amine groups
63	CM	metal binding imine and phenol centers
65	CM	Metalated porphyrin sites
48	CH	amino and triazine groups to form H-bonds
69	PN	thioether metal binding sites in the cavity
28, 29, 70-73	PN	diamine metal binding sites

Note: DCvC: dynamic covalent chemistry; CC: coordination chemistry; SOC: synthetic organic chemistry; CP: cage-to-polymer; CO: cage-to-ordered organic framework; CM: cage-to-MOF; CH: cage-to-HOF; PN: POC-nanoparticle

Summary and outlook

Post-synthetic modification[49] of POCs has rapidly emerged as an innovative strategy for improving the function-added values of POCs and engineering their properties and functions. A wide range of cage-based functional materials including porous cage-frameworks, cage-nanoparticle composites, and cage-salt electrolyte composites have been developed through post-synthetic modification of POCs. The use of POCs as nanosized synthons offers novel materials with unusual structure features,

chemical stability, and functions, such as guest-binding capacity and selectivity, sensing capability, and catalytic efficiency, which cannot be easily achieved otherwise. This tutorial review summarizes the PSM strategies utilizing dynamic covalent chemistry, coordination synthetic chemistry, synthetic organic chemistry, supramolecular chemistry, nanotechnology, or their combinations, which have enabled the enrichment of POCs materials by accessing novel cage, porous liquid, frameworks, and composites with unprecedented physicochemical functionalities, Table 1.

Although tremendous progress has been made, the continuous development of POC-based materials is still facing significant challenges: (1) the limited synthetic topology for POCs represents a bottleneck in developing chemically stable and POC-based functional materials through PSM. Most reported POCs are highly symmetrical polyhedra. POCs with low-symmetry structures would have multiple different types of pore windows, which could bring interesting properties for molecular separation and catalysis, etc. (2) More simple-to-make functional POCs should be developed to enable large scale preparation/fabrication of materials and devices through PSM for practical applications. (3) Rational design principles and novel synthetic approaches for modification of POCs should be further developed to expand the functional diversity of POC-based materials. For example, integrating functional guests (e.g., molecular catalyst) noncovalently/covalently into POCs through PSM would be a promising direction to discover advanced multi-component systems with functional synergy. Functional organic spacers connecting POCs could also play an important role in engineering the properties of covalent POC assemblies, such as the electron excitation/transportation, porosity, and structure flexibility. (4) Strategies for controlling the intercage porosity through PSM should be developed. The covalent crosslinking of POCs through simultaneous polymerization and crystallization using dynamic covalent chemistry should be further developed to form ordered frameworks with controlled porosity rather than amorphous polymers. Moreover, the large families of POCs connected with different organic spacers but with the same structural topology should be explored using reticular chemistry as commonly seen in COF synthesis, which could tune the size and chemical environment of the pores. As alternative approaches, molecular and crystal engineering strategies could be exploited to achieve fine tuning of exterior intercage voids. (5) PSM of POCs should be considered for integration into the device fabrication to effectively strengthen surface uniformity and interface contact. (6) Electrochemical investigation on POC-based materials has rarely been explored due to their relatively low conductivity and the lack of electrocatalytic active sites. PSM could direct the covalent connection of POCs with electronic substrate (such as electron conductive carbon materials), facilitating the electron transfer. Given the great progress achieved in PSM of POCs within the past ten years or so, we believe continuous exploitation over diverse applications of POC-based materials would lead to a much booming perspective in this rapidly growing field.

Conflicts of interest

There are no conflicts to declare.

Acknowledgements

The work was supported by the National Natural Science Foundation of China (Nos. 21631003 and 21805005), Fundamental Research Funds for the Central Universities (Nos. FRF-BD-20-14A, FRF-IDRY-19-028 and FRF-BR-19-003B), University of Science and Technology Beijing, University of Colorado Boulder, and NSF (DMR-1420736).

Notes and references

1 J. R. Holst, A. Trewin and A. I. Cooper, *Nat. Chem.*, 2010, **2**, 915-920.
2 G. Zhang and M. Mastalerz, *Chem. Soc. Rev.*, 2014, **43**, 1934-1947.
3 R. D. Mukhopadhyay, Y. Kim, J. Koo and K. Kim, *Acc. Chem. Res.*, 2018, **51**, 2730-2738.
4 E. J. Dale, N. A. Vermeulen, A. A. Thomas, J. C. Barnes, M. Jurícek, A. K. Blackburn, N. L. Strutt, A. A. Sarjeant, C. L. Stern, S. E. Denmark and J. F. Stoddart, *J. Am. Chem. Soc*. 2014, **136**, 10669-10682.
5 P.-E. Alexandre, W.-S. Zhang, F. Rominger, S. M. Elbert, R. R. Schrçder and M. Mastalerz, *Angew. Chem., Int. Ed*., 2020, **59**, 19675-19679.
6 C. Liu, K. Liu, C. Wang, H. Liu, H. Wang, H. Su, X. Li, B. Chen and J. Jiang, *Nat. Commun.,* 2020, **11**, 1047.
7 L. Chen, P. S. Reiss, S. Y. Chong, D. Holden, K. E. Jelfs, T. Hasell, M. A. Little, A. Kewley, M. E. Briggs, A. Stephenson, K. M. Thomas, J. A. Armstrong, J. Bell, J. Busto, R. Noel, J. Liu, D. M. Strachan, P. K. Thallapally and A. I. Cooper, *Nat. Mater*., 2014, **13**, 954-960.
8 L. Zhang, Y. Jin, G.-H. Tao, Y. Gong, Y. Hu, L. He and W. Zhang, *Angew. Chem., Int. Ed*., 2020, **59**, 20846-20851.
9 S. J. Rowan, S. J. Cantrill, G. R. L. Cousins, J. K. M. Sanders and J. F. Stoddart, *Angew. Chem. Int. Ed.*, 2002, **41**, 898-952.
10 Y. Jin, C. Yu, R. J. Denman and W. Zhang, *Chem. Soc. Rev.*, 2013, **42**, 6634-6654.
11 P. T. Corbett, J. Leclaire, L. Vial, K. R. West, J. L. Wietor, J. K. M. Sanders and S. Otto, *Chem. Rev.*, 2006, **106**, 3652-3711.
12 R. L. Greenaway, V. Santolini, M. J. Bennison, B. M. Alston , C. J. Pugh, M. A. Little, M. Miklitz, E. G. B. Eden-Rump, R. Clowes, A. Shakil, H. J. Cuthbertson, H. Armstrong, M. E. Briggs, K. E. Jelfs and A. I. Cooper, *Nat. Commun*., 2018, **9**, 2849.
13 T. Hasell, X. F. Wu, J. T. A. Jones, J. Bacsa, A. Steiner, T. Mitra, A. Trewin, D. J. Adams and A. I. Cooper, *Nat. Chem.*, 2010, **2**, 750-755.
14 G. Zhang, O. Presly, F. White, I. M. Oppel and M. Mastalerz, *Angew. Chem. Int. Ed.*, 2014, **53**, 5126-5130.
15 Q. Wang, C. Yu, H. Long, Y. Du, Y. H. Jin and W. Zhang, *Angew. Chem. Int. Ed.*, 2015, **54**, 7550-7554.
16 C. J. Pugh, V. Santolini, R. L. Greenaway, M. A. Little, M. E. Briggs, K. E. Jelfs and A. I. Cooper, *Crystal Growth & Design*, 2018, **18**, 2759-2764.
17 K. Acharyya, S. Mukherjee and P. S. Mukherjee, *J. Am. Chem. Soc.*, 2013, **135**, 554-557.
18 S. Akine, M. Miyashita and T. J. Nabeshima, *Am. Chem. Soc.*, 2017, **139**, 4631-4634.
19 P. T. Smith, Y. Kim, B. P. Benke, K. Kim and C. J. Chang, *Angew. Chem. Int. Ed.*, 2020, **59**, 4902-4907.
20 P. T. Smith, B. P. Benke, Z. Cao, Y. Kim, E. M. Nichols, K. Kim and C. J. Chang, *Angew. Chem. Int. Ed.*, 2018, **57**, 9684-9688.

21 Y. Jin, B. A. Voss, R. D. Noble and W. Zhang, *Angew. Chem. Int. Edit.*, 2010, **49**, 6348-6351.
22 M. Liu, M. A. Little, K. E. Jelfs, J. T. A. Jones, M. Schmidtmann, S. Y. Chong, T. Hasell and A. I. Cooper, *J. Am. Chem. Soc.*, 2014, **136**, 7583-7586.
23 M. Liu, L. D. Zhang, M. A. Little, V. Kapil, M. Ceriotti, S. Y. Yang, L. F. Ding, D. L. Holden, R. Balderas-Xicohtencatl, D. L. He, R. Clowes, S. Y. Chong, G. Schutz, L. J. Chen, M. Hirscher and A. I. Cooper, *Science*, 2019, **366**, 613-620.
24 M. W. Schneider, I. M. Oppel, A. Griffin and M. Mastalerz, *Angew. Chem. Int. Ed.*, 2013, **52**, 3611-3615.
25 A. S. Bhat, S. M. Elbert, W. S. Zhang, F. Rominger, M. Dieckmann, R. R. Schroder and M. Mastalerz, *Angew. Chem. Int. Ed.*, 2019, **58**, 8819-8823.
26 Q. Q. Wang, N. Luo, X. D. Wang, Y. F. Ao, Y. F. Chen, J. M. Liu, C. Y. Su, D. X. Wang and M. X. Wang, *J. Am. Chem. Soc.*, 2017, **139**, 635-638.
27 Y. Jin, B. A. Voss, R. McCaffrey, C. T. Baggett, R. D. Noble and W. Zhang, *Chem. Sci.*, 2012, **3**, 874-877.
28 Z. Wang, H. Ma, T. L. Zhai, G. Cheng, Q. Xu, J. M. Liu, J. K. Yang, Q. M. Zhang, Q. P. Zhang, Y. S. Zheng, B. Tan and C. Zhang, *Adv. Sci.*, 2018, **5**, 1800141.
29 M. J. Kory, M. Worle, T. Weber, P. Payamyar, S. W. van de Poll, J. Dshemuchadse, N. Trapp and A. D. Schluter, *Nat. Chem.*, 2014, **6**, 779-784.
30 J. X. Ma, J. Li, Y. F. Chen, R. Ning, Y. F. Ao, J. M. Liu, J. L. Sun, D. X. Wang and Q. Q. Wang, *J. Am. Chem. Soc.*, 2019, **141**, 3843-3848.
31 Q. Zhu, X. Wang, R. Clowes, P. Cui, L. Chen, M. A. Little and A. I. Cooper, *J. Am. Chem. Soc.*, 2020, **142**, 16842-16848.
32 Z. Shan, X. Wu, B. Xu, Y. l. Hong, M. Wu, Y. Wang, Y. Nishiyama, J. Zhu, S. Horike, S. Kitagawa and G. Zhang, *J. Am. Chem. Soc.*, 2020, **142**, 21279-21284.
33 M. O'Keeffe and O. M. Yaghi, *Chem. Rev.,* 2012, **112**, 675-702.
34 R.-B. Lin, Y. He, P. Li, H. Wang, W. Zhou and B. Chen, *Chem. Soc. Rev.,* **2019**, *48*, 1362-1389.
35 S. I. Swamy, J. Bacsa, J. T. A. Jones, K. C. Stylianou, A. Steiner, L. K. Ritchie, T. Hasell, J. A. Gould, A. Laybourn, Y. Z. Khimyak, D. J. Adams, M. J. Rosseinsky and A. I. Cooper, *J. Am. Chem. Soc.*, 2010, **132**, 12773-12775.
36 L. Zhang, L. Xiang, C. Hang, W. L. Liu, W. Huang and Y. C. Pan, *Angew. Chem. Int. Ed.*, 2017, **56**, 7787-7791.
37 Y. Kim, J. Koo, I. C. Hwang, R. D. Mukhopadhyay, S. Hong, J. Yoo, A. A. Dar, I. Kim, D. Moon, T. J. Shin, Y. H. Ko and K. Kim, *J. Am. Chem. Soc.*, 2018, **140**, 14547-14551.
38 B. Han, H. L. Wang, C. M. Wang, H. Wu, W. Zhou, B. L. Chen and J. Z. Jiang, *J. Am. Chem. Soc.*, 2019, **141**, 8737-8740.
39 K. C. Jie, N. Onishi, J. A. Schott, I. Popovs, D. E. Jiang, S. Mahurin and S. Dai, *Angew. Chem. Int. Ed.*, 2020, **59**, 2268-2272.
40 R. McCaffrey, H. Long, Y. H. Jin, A. Sanders, W. Park and W. Zhang, *J. Am. Chem. Soc.*, 2014, **136**, 1782-1785.
41 L. Qiu, R. McCaffrey, Y. H. Jin, Y. Gong, Y. M. Hu, H. L. Sun, W. Park and W. Zhang, *Chem. Sci.*, 2018, **9**, 676-680.
42 J.-K. Sun, W.-W. Zhan, T. Akita and Q. Xu, *J. Am. Chem. Soc.*, 2015, **137**, 7063-7066.
43 X.-C. Yang, J.-K. Sun, M. Kitta, H. Pang and Q. Xu, *Nat. Catal.*, 2018, **1**, 214-220.
44 B. Mondal, K. Acharyya, P. Howlader and P. S. Mukherjee, *J. Am. Chem. Soc.*, 2016, **138**, 1709-1716.
45 N. N. Sun, C. M. Wang, H. L. Wang, L. Yang, P. Jin, W. Zhang and J. Z. Jiang, *Angew. Chem. Int. Ed.*, 2019, **58**, 18011-18016.
46 M. Nihei, H. Ida, T. Nibe, A. M. P. Moeljadi, Q. T. Trinh, H. Hirao, M. Ishizaki, M. Kurihara, T. Shiga and H. Oshio, *J. Am. Chem. Soc.*, 2018, **140**, 17753-17759.
47 M. Liu, L. J. Chen, S. Lewis, S. Y. Chong, M. A. Little, T. Hasell, I. M. Aldous, C. M. Brown, M. W. Smith, C. A. Morrison, L. J. Hardwick and A. I. Cooper, *Nat. Commun.*, 2016, **7**, 12750.
48 A. Petronico, T. P. Moneypenny, B. G. Nicolau, J. S. Moore, R. G. Nuzzo and A. A. Gewirth, *J. Am. Chem. Soc.*, 2018, **140**, 7504-7509.
49 D. A. Roberts, B. S. Pilgrim and J. R. Nitschke, *Chem. Soc. Rev.*, 2018, **47**, 626-644.